The influence of Caribbean Current eddies on coastal circulation in the Southwest Caribbean Sea

S.E. Kastner,[a] G. Pawlak,[b,c] S. N. Giddings,[c] A. E. Adelson, [c] R. Collin, [d] K. A. Davis[e]

[a] *Western Washington University, Department of Environmental Science, Bellingham, WA, USA*

[b] *Department of Mechanical and Aerospace Engineering, University of California - San Diego, San Diego, CA, USA* [c] *Scripps Institution of Oceanography, University of California - San Diego, San Diego, CA, USA* [d] *Smithsonian Tropical Research Institute, Balboa Ancon, Panamá*

[e] *Department of Civil & Environmental Engineering, University of California - Irvine, Irvine, CA, USA*

Corresponding author: Samuel E. Kastner, sam.kastner@wwu.edu

Early Online Release: This preliminary version has been accepted for publication in *Journal of Physical Oceanography*, may be fully cited, and has been assigned DOI 10.1175/JPO-D-24-0049.1. The final typeset copyedited article will replace the EOR at the above DOI when it is published.

ABSTRACT: Westward-propagating Caribbean Current eddies modify the volume-integrated potential vorticity (PV) balance in the western Caribbean Sea, influencing the circulation of the Panamá-Colombia Gyre (PCG) and of coastal currents hundreds of kilometers to the south of the eddies' mean trajectory. Using 22 years of output from the Hybrid Coordinate Ocean Model, we apply a volume-integrated eddy phase-averaged 1.5 layer PV balance, showing that PV fluxes into the PCG region are balanced by frictional PV dissipation represented by linear drag along the coastline. Coastal currents in the PCG region vary by a factor of two in phase with the passage of a Caribbean Current eddy over the 116 day average eddy period. Flow separation at the Isthmus of Panamá results in a vortex shed from Darien Gulf, which slows the coastal currents in the gyre region from their maximum during eddy events. An annual ensemble average PV balance in the gyre region shows that the mean PV influx to this region is higher from August to October. Correspondingly, the range of coastal currents in the gyre region over an eddy event is modestly influenced by the PV influx magnitude. Eddy influenced reversals in the coastal current can occur between November and July at Bocas del Toro and year-round at Colón. Such coastal current reversals are important for alonghshore transport of larvae, freshwater, and chemical tracers.

Accepted for publication in *Journal of Physical Oceanography*. DOI 10.1175/JPO-D-24-0049.1.

1. Introduction

Anti-cyclonic eddies are a dominant feature of the Caribbean Current as it passes through the northwest Caribbean Sea. In this work, we will show that such eddies significantly influence flow features in the southwest Caribbean Sea, namely, the Panamá-Colombia Gyre and the Caribbean Coastal Countercurrent. This remotely forced influence is an important mechanism for coastal current variability along the Caribbean south coast from Costa Rica to Colombia.

We refer to three types of rotational flow structures in this work, and we use different nomenclature to refer to each structure. Caribbean Current eddies, anticyclonic features that propagate westward across the northern Caribbean Sea, will be referred to as "eddies" where their full name is not used. The Panamá-Colombia Gyre, a cyclonic stationary feature in the southwestern Caribbean Sea, will be referred to as either the "PCG" or the "gyre". The anticyclonic circulation that occasionally forms in the Darien Gulf will be referred to as a "vortex".

Caribbean Current eddies propagate westward across the Caribbean Sea, advected by the Current's mean westward geostrophic flow (Andrade and Barton 2000; Centurioni and Niiler 2003; Richardson 2005). Some Caribbean Current eddies propagate into the Caribbean Sea as perturbations in the North Brazil Current (Huang et al. 2021), but many are locally generated via baroclinic instability mechanisms in the western Caribbean Sea, defined for this study as west of 73° W, as shown in Figure 1 (Andrade and Barton 2000; Jouanno et al. 2008, 2009; Lin et al. 2012; Orfila et al. 2021). The eddies take a few months to propagate across the basin, moving at speeds of 0.1 to 0.3 m/s (Andrade and Barton 2000; Jouanno et al. 2009), and have periods of roughly 120 days, the time scale on which a new eddy is either generated locally or propagates into the basin. This time scale is similar to a basin-wide oscillation mode (Lin et al. 2012; Hughes et al. 2016), although it is unknown if these mechanisms are connected.

The Caribbean Current eddies described above perturb the location and magnitude of maximum flow in the Caribbean Current. On average, the Caribbean Current propagates along the basin's northern side, passing north of the Central American Rise, where a shallow shelf extends far offshore of the coastline of Honduras and Costa Rica (Figure 1). As Caribbean Current eddies propagate westward across the Caribbean Sea basin, they shift the Caribbean Current maximum flow southwards, forcing the current to interact with the Central American Rise (Centurioni and Niiler 2003; Richardson 2005; Jouanno et al. 2008). This bathymetric interaction causes the eddies

Accepted for publication in *Journal of Physical Oceanography*. DOI 10.1175/JPO-D-24-0049.1.

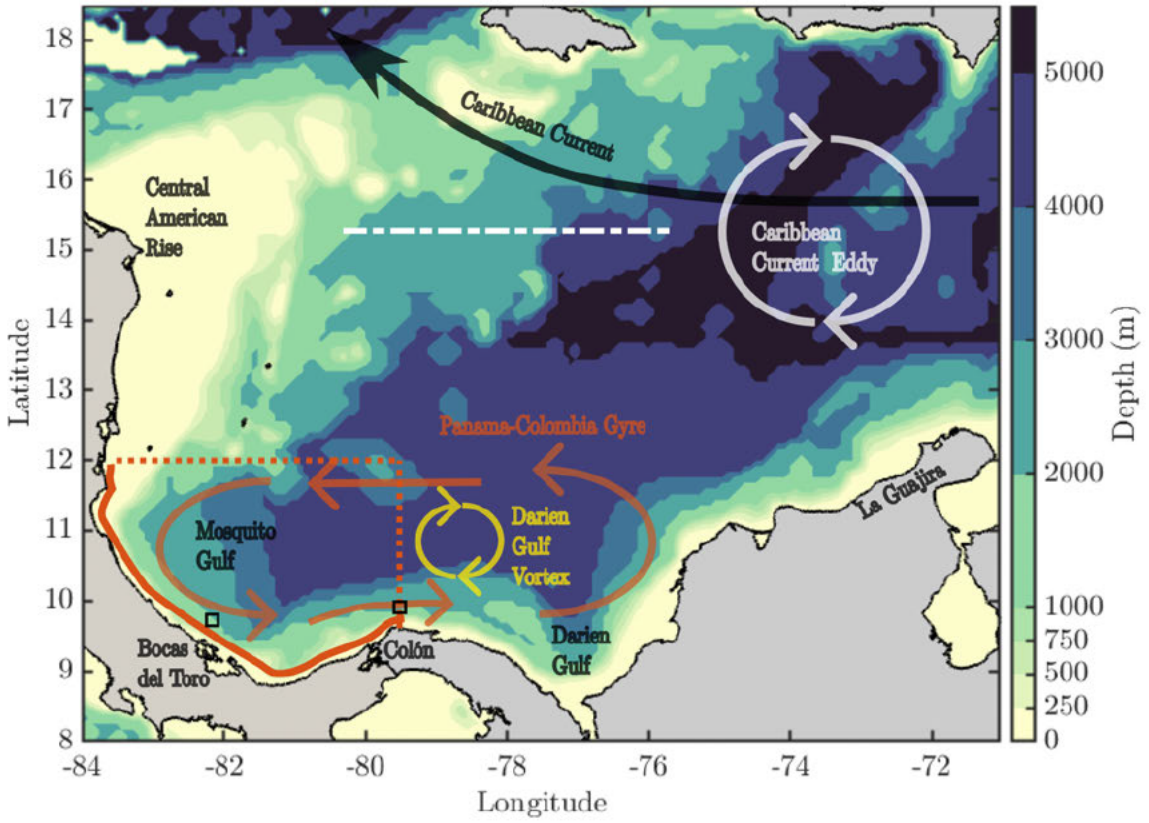

FIG. 1: HYCOM bathymetry in the western Caribbean Sea. Colors show depth in 250m increments to 1000m, and then 1000m increments to 5000m. The white dashed-dotted line in the northern part of the basin is the longitudinal transect used for phase averaging the vorticity fluxes in section 2d. Caribbean Current eddies, shown schematically in white, pass through the northern part of the basin along the average Caribbean Current path, shown in black. The orange lines in the southwestern part of the basin, Mosquito Gulf, delineate the control volume used for calculating the volume-integrated potential vorticity balance in section 3; the solid orange line denotes the closed coastal control volume boundary while the dashed orange lines denote the open control volume boundaries. The PCG sets up in this region (the orange arrows shown indicate mode (A) described in section 1). The Darien Gulf Vortex, shown in yellow, is the middle vortex described in mode (D). Locations chosen for coastal current analysis in subsequent sections for Bocas del Toro and Colón are shown as small black squares.

to break up (Andrade and Barton 2000; Lin et al. 2012), and forces flow to the south, where the Rossby wave energy contained by the Caribbean Current eddy field is converted to a barotropic mode (Hughes et al. 2016) and can interact with the persistent flow features of that region—the Caribbean Coastal Countercurrent and Panamá-Colombia Gyre.

The Caribbean Coastal Countercurrent (CCC) is a persistent eastward flow along the western Caribbean Sea's southern boundary, through the Mosquito Gulf (west of 80° W) along the Isthmus of Panamá's northern side, and then through the Darien Gulf (east of 79° W, Andrade et al. (2003); Lin et al. (2012); Correa-Ramirez et al. (2020); Orfila et al. (2021)). This current forms the

Accepted for publication in *Journal of Physical Oceanography*. DOI 10.1175/JPO-D-24-0049.1.

southern arm of the Panamá-Colombia Gyre (PCG), a cyclonic recirculation feature in the southwest Caribbean Sea (Mooers and Maul 1998; Andrade et al. 2003). The current is characterized by average velocities of $\sim 0.1 - 0.3$ m/s (Andrade et al. 2003; Correa-Ramirez et al. 2020). On the coast of Panamá, the CCC is maximum at the surface and occupies the upper 100m of the water column, while off La Guajira Peninsula, the current is maximum at depths of $\sim$ 200m. The CCC is a product of the Caribbean basin scale Sverdrup balance (Andrade et al. 2003), as such, it varies with the winds, intensifying during the upwelling season at La Guajira (Andrade et al. 2003; Correa-Ramirez et al. 2020). The CCC has been found to modify the source waters of the La Guajira Peninsula upwelling zone (Correa-Ramirez et al. 2020; Orfila et al. 2021), an ecologically unique region (Vasquez-Carrillo and Sullivan Sealey 2021).

Paired with the CCC are somewhat persistent westward flows between 10-14° N, forming the PCG's northern arm (Andrade et al. 2003; Lin et al. 2012; Correa-Ramirez et al. 2020; Orfila et al. 2021). We refer to these westward flows as only somewhat persistent because they exhibit variability in their zonal extent. The PCG's northern arm occasionally spans the entire width of the southwest Caribbean Basin; this is associated with strong flow in the CCC. This northern arm can be formed when the Caribbean Current is perturbed to the south by eddies (Lin et al. 2012). Notably, the PCG's northern arm often spans a shorter distance than the entire width of the southwest Caribbean Basin; it frequently only spans the northern boundary of Mosquito Gulf. In such cases, the circulation north of the Isthmus of Panamá and in the Darien Gulf is more complex, resulting in four previously observed PCG "modes": (A) a single cyclonic recirculation spanning the Mosquito and Darien Gulfs, (B) a single anti-cyclonic recirculation in the Darien Gulf, (C) two separate cyclonic recirculations, one each in the Mosquito and Darien Gulfs, or (D) an anti-cyclonic recirculation north of the Isthmus of Panamá paired with cyclonic recirculations in the Mosquito and Darien Gulfs (Andrade et al. 2003; Centurioni and Niiler 2003; Richardson 2005; Jouanno et al. 2008; Lin et al. 2012; Jouanno et al. 2012; Correa-Ramirez et al. 2020; Orfila et al. 2021). Mode (A) above corresponds to one single coherent recirculation spanning the entire southwest Caribbean, as shown by the orange arrows on Figure 1, while mode (B) corresponds to smaller area of circulation. Mode (C) accounts for two coherent vortices in the southwest Caribbean (one each in Mosquito Gulf and Darien Gulf), while mode (D) has three, adding a vortex north of the Isthmus of Panamá (this is the yellow vortex on Figure 1). Mode (A) has most frequently been

Accepted for publication in *Journal of Physical Oceanography*. DOI 10.1175/JPO-D-24-0049.1.

observed between July and October, while modes (B)-(D) are observed with equal frequency in the other months. This seasonal variability in mode (A) has been shown to be associated with seasonal variability in the Caribbean Low-Level Jet winds (Jouanno et al. 2012; Correa-Ramirez et al. 2020; Orfila et al. 2021). Variability on the shorter than seasonal time scales associated with Caribbean Current eddies has also been observed to be an important driver of variability in the PCG/CCC system (Jouanno et al. 2008; Lin et al. 2012).

Coherent, meso- to large-scale eddies have been shown to be important mechanisms for transport of heat, salt, energy, and momentum from western boundary currents to the coast. For example, Kuroshio eddies generate mass and salt fluxes in the South China Sea, thereby causing exchange of volume and salt (Yang et al. 2019). On the United States' southeastern coast, Gulf Stream eddies are associated with transport of nutrient rich water onto the shelf, and are therefore important for ecosystem productivity (Lee and Atkinson 1983; Yoder et al. 1981; Gaube and McGillicuddy 2017). Closer to the Caribbean Sea, frequent eddy shedding in the Gulf of Mexico Loop Current can modify the Gulf's salinity structure, and cause transport of freshwater through the Florida Straits (Schiller and Kourafalou 2014; Brokaw et al. 2019).

Coastal current variability, and particularly coastal current reversals, can be important to smaller scale processes and ecosystem dynamics (Brooks and Townsend 1989; Lee and Williams 1999; Siedlecki et al. 2015; Doblin and van Sebille 2016). Coastal currents have been shown to be important drivers of ecosystem connectivity (Roughan et al. 2011; Cowen et al. 2006). The direction and strength of coastal currents can also change nearshore water properties through upwelling or downwelling dynamics (Stone et al. 2018; Hickey et al. 2006). Coastal currents also interact with river plumes, influencing the transport pathways of terrestrial material and freshwater (Hickey et al. 2005; Horner-Devine et al. 2015).

Caribbean Current eddies are important sources of variability for alongshore currents on the coasts of Panamá, Costa Rica, and Colombia, 500 km south of the Caribbean Current's main branch. Previous studies have described this relationship by characterizing modes of variability (Jouanno et al. 2012; Lin et al. 2012) and resonance (Hughes et al. 2016) as described above. Here, we will use a dynamical approach in the form of a regional volume-integrated potential vorticity budget calculated with output from the Hybrid Coordinate Ocean Model, and phase-average to extract the eddy signal (section 2). We show that the PCG has a phase-dependent response to

Accepted for publication in *Journal of Physical Oceanography*. DOI 10.1175/JPO-D-24-0049.1.

Caribbean Current eddy passages, and that eddy phase-averaged vorticity fluxes are balanced by frictional vorticity spindown at the coastal boundary, which has implications for coastal current variability (section 3). We then discuss the timing and strength of Caribbean Current eddies relative to the annual cycles observed in previous work, and interpret the annual cycle to determine the periods when coastal currents are most likely to reverse (section 4).

2. Methods

a. HYCOM

We use output from the Hybrid Coordinate Ocean Model (HYCOM) Global Ocean Forecasting System (GOFS) 3.1 reanalysis product, GLBv0.08-53.X, run by the Naval Research Laboratory's Ocean Dynamics and Prediction Branch. This product contains 3 hourly global reanalysis output on a 1/12 degree resolution grid at 41 vertical levels (see the data availability statement for a link to the download portal) (Chassignet et al. 2007). Model output is available from 1994-2015. Two versions of the National Centers for Environmental Prediction (NCEP) Climate Forecast System Reanalysis (CFSR) are used for surface forcing; version 1 is used from 1994-2010, version 2 is used from 2011 onward (Saha et al. 2010, 2014). Data assimilation for this reanalysis uses the Navy Coupled Ocean Data Assimilation (NCODA) system; this system makes use of satellite altimetry and temperature measurements as well as in situ temperature and salinity measurements such as expendable bathythermographs (XBTs) and Argo floats (Cummings 2005; Cummings and Smedstad 2013).

HYCOM products are commonly used in studies of meso- and larger scale processes (Wilson and Riser 2016; Putman et al. 2018; Orfila et al. 2021). Our region of interest for this study spans from 8-18.5°N and 71-84°W. Our analysis uses a 1.5 layer model with an active surface layer (Section 2b); HYCOM's vertical resolution is variable, with 2m resolution near the surface increasing to 50m resolution by 350m depth.

b. 1.5 layer model approximation

The processes described in Section 1 all occur in the surface layer of the Caribbean Sea; in order to represent them simply, we define a 1.5 layer model that includes an active surface layer overlying a higher density, inactive lower layer (Yang and Price 2000; Pratt et al. 2019). We define

Accepted for publication in *Journal of Physical Oceanography*. DOI 10.1175/JPO-D-24-0049.1.

the surface layer as the depth at which $\rho = 1026.36$ kg/m^3. This density cutoff was determined by first taking the spatial average density and kinetic energy at all HYCOM depth bins within the PCG region shown on Figure 1. Here we define the kinetic energy as $KE = \frac{1}{2}(u^2 + v^2)$, where u is the zonal and v is the meridional velocity. We then find the e-folding depth of KE ($\sim$ 125 m) and the associated density. This choice of isopycnal therefore represents the relevant surface layer for the processes outlined in section 1. Performing the same analysis in the main trunk of the Caribbean Current (between 76-81 °W and 14-17.5 °N) yields a larger e-folding depth ($\sim$ 175 m), but a similar isopycnal ($\rho = 1026.36$ kg/m^3). Using the kinetic energy at one standard deviation higher and lower than the mean in both regions (PCG and Caribbean Current) yields a range of densities for the gyre ($1026.16 < \rho < 1026.43$ kg/m^3) and the Caribbean Current ($1026.21 < \rho < 1026.86$ kg/m^3). The similarity between regions of the isopycnals associated with the e-folding depths from the mean kinetic energy indicates that this choice of isopycnal is a reasonable determination of the surface layer throughout the western Caribbean Sea.

We calculate the surface layer depth, H, and depth averages of zonal and meridional velocity using the 1026.36 kg/m^3 isopycnal boundary for the domain shown in Figure 1 over the 22 year record of GLBv0.08-53.X output. We use vertical linear interpolation to approximate layer depths and layer average velocities on a finer vertical resolution than HYCOM's grid spacing (at least 25m below 100m depth). We then apply a low pass filter to the layer depth, layer-averaged velocity, layer-averaged density, and sea surface height using a filter window of the maximum inertial period in the domain shown on Figure 1, $T_i \approx 86$ hrs. This filtering window smooths over inertial oscillations and the HYCOM data assimilation time scale (1 day) for the entire domain. All calculations presented in the rest of this work use these low-pass filtered quantities.

c. Vorticity calculations

We calculate potential vorticity (PV) in the active surface layer defined in Section 2b as

$$Q = \frac{\zeta + f}{H}, \tag{1}$$

where the local vorticity $\zeta = \frac{\partial v}{\partial x} - \frac{\partial u}{\partial y}$ is defined using surface layer average velocity components; u and v, in the zonal direction, x, and the meridional direction, y, respectively. In equation 1, f is the local Coriolis parameter, which varies from 2.02×10^{-5} s^{-1} at 8.5°N to 4.62×10^{-5} s^{-1} at

Accepted for publication in *Journal of Physical Oceanography*. DOI 10.1175/JPO-D-24-0049.1.

18.5°N (we do not use a β-plane approximation), and H is the surface layer depth calculated in Section 2b (Vallis 2006).

PV is a conserved quantity; changes in Q along a streamline can only be caused by external PV fluxes such that

$$\frac{DQ}{Dt} = \mathcal{F} - \mathcal{D}, \tag{2}$$

where D/Dt indicates the material derivative, $\mathcal{F}$ indicates all external sources of PV, and $\mathcal{D}$ indicates all external sinks of PV (Rhines 1986). Here, we assume that $\mathcal{F}$ is equivalent to the wind stress curl, and that $\mathcal{D}$ is equivalent to the frictional dissipation of PV. Integrating equation 2 over the PCG region control volume defined by the orange lines on Figure 1, assuming that the stress on the ocean surface is only due to the wind, and assuming that stress on the control volume's bottom is only due to linear drag yields the volume-integrated potential vorticity (PV) balance,

$$\underbrace{\iint \frac{\partial QH}{\partial t} dA}_{\text{PV storage}} + \underbrace{\int_{\text{open bound.}} QH\vec{u}\cdot\hat{n}ds}_{\text{Net PV flux}} = \underbrace{\iint \frac{1}{\rho H}\left(\frac{\partial \tau_y}{\partial x} - \frac{\partial \tau_x}{\partial y}\right) dA}_{\text{wind stress curl}} - \underbrace{\iint r\zeta dA}_{\text{linear friction}}, \tag{3}$$

where $dA = dxdy$ indicates an integral over the control volume plan-form area, dx and dy indicate integrals taken in the zonal and meridional directions, ρ is the laterally variable surface layer averaged density, τ_x and τ_y are the zonal and meridional wind stress components respectively, and r is a linear coefficient of friction. For the remainder of the manuscript, we consider the volume-integrated PV balance and its associated flux terms. For the sake of brevity, we will describe these simply as the "PV balance" and its associated "PV fluxes". Advective PV flux through the bottom of the control volume is zero: the bottom surface is an isopycnal and is therefore impermeable to such fluxes (Bretherton and Schär 1993; Marshall 2000). Thermodynamic PV fluxes due to surface heating and diapycnal turbulent mixing through the bottom isopycnal (Haynes and McIntyre 1987; Marshall 2000) are found to be orders of magnitude smaller than the horizontal advective fluxes in a scaling analysis (not shown) and are therefore omitted from consideration in equation 2. Each of the four terms in equation 3 are discussed in more detail below.

The change of surface layer PV in time within the volume, or PV storage, is calculated as shown in the first term on the left hand side of equation 3. This formulation allows both Q and H to vary in time. We can estimate the PV flux into a volume in the zonal and meridional directions as the

Accepted for publication in *Journal of Physical Oceanography*. DOI 10.1175/JPO-D-24-0049.1.

second term in equation 3, where ds indicates that the integral is taken along the open boundaries of the control volume. In the active surface layer average framework for the open boundaries of the control volume shown in dashed orange on Figure 1,

$$\underbrace{\int_{\text{open bound.}} QH\vec{u}\cdot\hat{n}ds}_{\text{Net PV flux}} = \underbrace{\int_{\text{E. boundary}} QHudy}_{\text{zonal flux}} + \underbrace{\int_{\text{N. boundary}} QHvdx}_{\text{meridional flux}}, \tag{4}$$

where "E. boundary" and "N. boundary" indicate the control volume eastern and northern boundaries, respectively, through which the advective flux terms act (see Figure 1).

The influence of wind on vorticity is quantified using the HYCOM's NCEP CSFR forcing (or CSFv2, depending on the year, as described in section 2a). The CFSR wind stress product is low-pass filtered at the same cutoff as the HYCOM output and interpolated onto the 1/12 degree resolution HYCOM grid. The vertical wind stress curl is calculated as the integral over the control volume's ocean surface face as in the first term on the right hand side of equation 3 (Vallis 2006).

We use Stokes' Theorem to transform the bottom stress area integral in equation 3 to a line integral around the outside of the control volume. Additionally, we assume that the linear coefficient of friction, r, is well represented by one constant, r_c, along the coast (solid orange line on Figure 1) and another constant, r_o, along the domain's open boundaries (dashed orange line on Figure 1). Out approach does not explicitly account for horizontal turbulent transport processes, and so we expect that some influence of lateral drag will be captured by this analysis. This methodology is similar to that used by Yang and Price (2000) and Chang and Oey (2011), but adapted for an active surface layer rather than a bottom layer. Along the coast, the frictional PV dissipation is taken to be due to the bottom stress because the surface layer of interest intersects the bed, while along the open boundaries, frictional PV dissipation is due to interfacial stress between the surface layer and the water below it (although we again note the influence of lateral drag in both terms). This yields:

$$\iint r\zeta dA = \underbrace{r_c \int_{\text{coast}} \vec{u}\cdot d\vec{s}}_{\text{coastal friction}} + \underbrace{r_o \int_{\text{open}} \vec{u}\cdot d\vec{s}}_{\text{open-boundary friction}}, \tag{5}$$

Accepted for publication in *Journal of Physical Oceanography*. DOI 10.1175/JPO-D-24-0049.1.

where $d\vec{s}$ is the unit vector in the counter-clockwise direction. To calculate the integral $\int_{\text{coast}} \vec{u} \cdot d\vec{s}$, we identify the HYCOM grid cells where the surface layer extends to within 25m of the seabed, including the tolerance factor of 25m to account for the model's coarse vertical spacing at depths greater than 100m. The locations chosen with this method do not vary significantly with time; due to the relative stability of the coastal surface layer depth and steep continental slope, this method approximates the shape of the coastline. We fit a cubic spline in space to these locations and interpolate the filtered, surface layer averaged velocity from the HYCOM grid onto the spline-fit locations. We then take the path integral of the along-path component of the interpolated velocity field along the spline-fit locations.

We seek to determine the constants r_c and r_o using a linear fit, where the sum of the PV storage, net PV flux, and negative wind stress curl terms in equation 3 is the response variable and the linear friction term is the predictor, using the formulation in equation 5 (moving the wind stress curl to the left hand side of equation 3). However, as the path integrals of velocity along the coast and the open boundaries oscillate in phase (see section 3a), a unique solution for r_c and r_o is not possible through linear fitting. Since we expect that the open boundary friction term in equation 5 will be small relative to the coastal friction term, as in Yang and Price (2000) and Chang and Oey (2011), we will approximate the average effects of open boundary friction as a constant, C, which allows us to use a linear fit to approximate r_c. Mathematically, we assume that

$$C \approx -r_o \overline{\int_{\text{open}} \vec{u} \cdot d\vec{s}}, \tag{6}$$

where the overbar indicates the average of the line integral of velocity along the open boundary over all eddy phases. This formulation assumes that interfacial friction is the only source or sink of PV that contributes to the constant, C, and yields a single value of r_o, presented in section 3b. An additional complication of this fitting method is that sources or sinks of vorticity that vary in phase with the along-coast velocity, such as lateral drag, will be included within bottom drag in r_c (see also section 3b). Combining equations 4-6 with equation 3, and moving the wind stress curl term to the left hand side, we may therefore rewrite the control volume PV budget as

Accepted for publication in *Journal of Physical Oceanography*. DOI 10.1175/JPO-D-24-0049.1.

$$\underbrace{\iint \frac{\partial QH}{\partial t} dA}_{\text{storage}} + \underbrace{\int_{\text{E. bound.}} QHu dy}_{\text{zonal flux}} + \underbrace{\int_{\text{N. bound.}} QHv dx}_{\text{meridional flux}} - \underbrace{\iint \frac{1}{\rho H}\left(\frac{\partial \tau_y}{\partial x} - \frac{\partial \tau_x}{\partial y}\right) dA}_{\text{wind stress curl}} = \underbrace{-r_c \int_{\text{coast}} \vec{u} \cdot d\vec{s}}_{\text{coastal friction}} + C, \tag{7}$$

the form of the PV balance used in section 3.

d. Phase averaging

To assess the influence of Caribbean Current eddies on the western Caribbean Sea broadly, we phase-average with respect to the eddies' east-to-west propagation across the basin. To define the eddy phase, we calculate the total meridional PV flux integrated along the 15.25°N line of latitude (shown in Figure 1 as a dashed white line), extending from 75.5 to 80.5°W. This integrated meridional PV flux is low-pass filtered (40 day window) to facilitate detection of longer period eddy events. An eddy event begins when the integrated, filtered, meridional PV flux crosses from below to above its mean value over the entire 22 year record (Figure 2, dashed black lines indicate these up-crossings), 1.11 m^2/s^2. The event ends upon the next recurrence of this condition. This method is similar to other oceanographic studies that make use of phase-averaging (Pawlak and MacCready 2002; McCabe et al. 2006; Nidzieko and Monismith 2013; Arzeno et al. 2020; Harvey et al. 2023). During the 22 year HYCOM record, we detect 66 eddies with an average period of T_{eddy}=116 days with a standard deviation of 31.5 days (roughly 3 eddies per year). Here, we define eddy period as the duration of the eddy event detected. This is similar to previously reported values of Caribbean Current eddy period using different methodology (Andrade and Barton 2000; Lin et al. 2012; Jouanno et al. 2012), and notably similar to the resonant period of 120 days identified by Hughes et al. (2016). We do not include eddy events with periods more than two standard deviations away from the mean; this excludes two eddy events with durations longer than 190 days. The minimum eddy period used in our subsequent work is 62.5 days. The maximum eddy period used is 172.4 days.

Our results are not sensitive to the length of the line chosen for integration, and are only mildly sensitive to whether the line is oriented zonally (as described) or meridionally. Varying the length from ~ 10 to ~ 1000 km yielded similar numbers of eddies (within 15%) and similar eddy durations

Accepted for publication in *Journal of Physical Oceanography*. DOI 10.1175/JPO-D-24-0049.1.

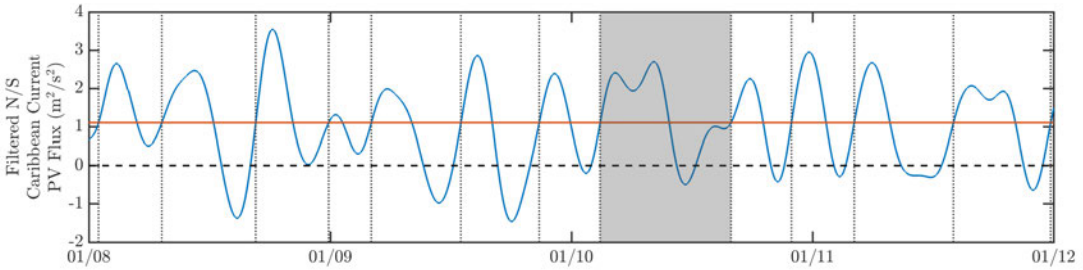

FIG. 2: A subsample (~ 4 of the 22 years) of the time series of low-pass filtered meridional PV flux through the white line on Figure 1. The orange line shows the mean value of this PV flux, the dotted black lines show the boundaries of each eddy detection. The grey area shows an eddy with a period of 198 days that was not included in the analysis.

(within 5%) to the results presented below. Additionally, using the integrated meridional PV flux along a north-south line at 75.5°W, extending from 13 to 17.5°N, yields similar eddy statistics to those presented above (78 eddies with an average period of 102 days for the same length line).

We calculate a phase-average of various quantities of interest, normalizing by the eddy duration, so that shorter eddies and longer eddies have an equal effect on the phase-average. We perform the phase-average in 5 degree bins, corresponding to approximately 1.5 days for the average eddy period. We calculate the phase-average of properties such as east velocity, north velocity, sea surface height (η or SSH), and surface layer depth, as well as the phase-average of calculations made with those properties, such as advective PV fluxes, PV storage, wind stress curl, and integrated along-coast velocity (section 2c, equation 7). Variability with phase of the phase-averaged quantities may thus be interpreted as the effect of the passage of a Caribbean Current eddy through the northern part of the Caribbean Sea. We examine the resulting phase-averaged PV balance in section 3b.

3. Eddy phase-average results

a. Phase-averaged structure of Caribbean Current eddies

Phase-averages of Q, ζ, H, and η calculated using the method outlined in section 2d allow us to characterize the passage of eddies in the Caribbean Current and the western Caribbean Sea's average response to those eddies (Figure 3). Supplemental video 1 shows the same information as Figure 3 for finer (5°) phase increments. Caribbean Current eddies have, on average, a negative local vorticity (anti-cyclonic), larger H than the surrounding surface layer, and a positive SSH. This combination leads eddy phase-averaged PV to be positive as the Coriolis parameter tends to be of equal or greater magnitude to the local vorticity (equation 1). The PV anomaly reflects patterns

Accepted for publication in *Journal of Physical Oceanography*. DOI 10.1175/JPO-D-24-0049.1.

seen in the local vorticity where the Caribbean Current eddies have lower PV than the background system PV (not shown). The superposition of the westward propagating eddy's negative vorticity and the Caribbean Current mean flow leads to stronger westward currents in the southern Caribbean current, and weaker eastward currents in the northern Caribbean current.

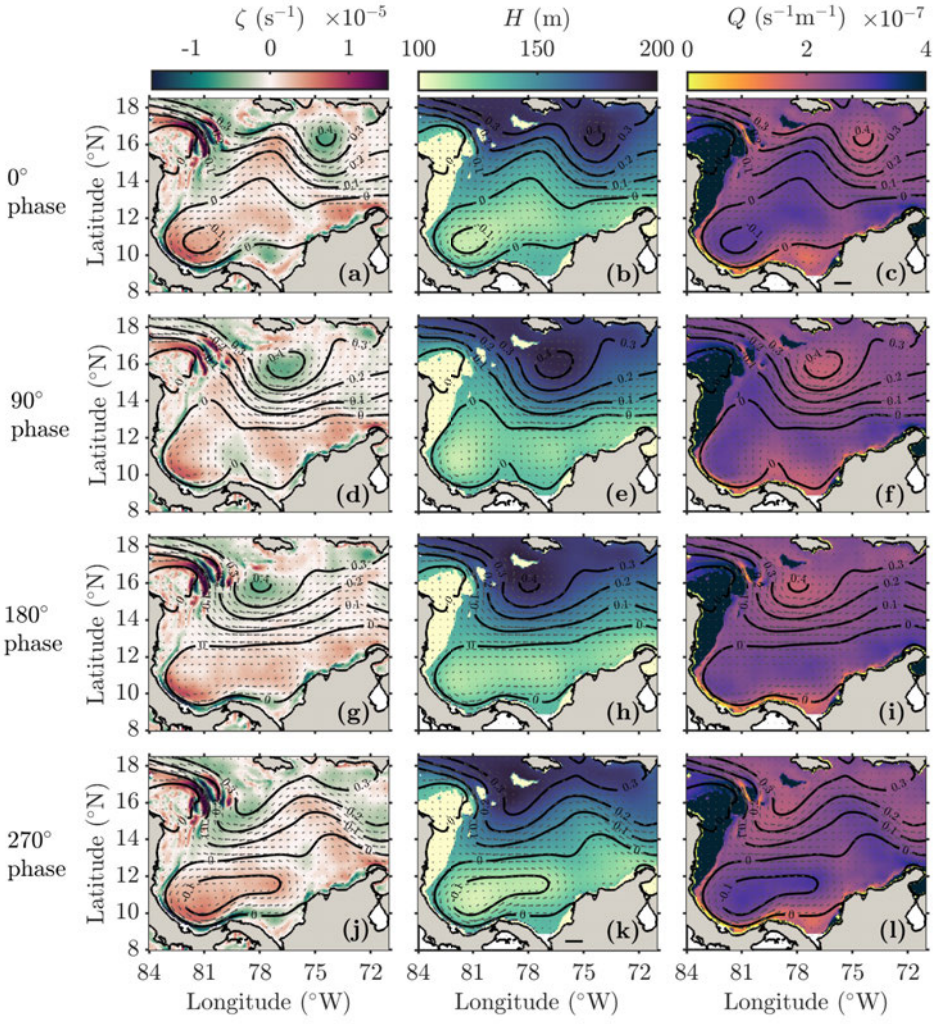

FIG. 3: Evolution of a phase-averaged eddy. On all subplots, vectors show the surface layer averaged velocity field (0.5 m/s scale arrow located at 76° W on panel c) and solid black lines show sea surface height contours in 0.1 m increments. Panels (a)-(c) show the eddy at 0° phase, (d)-(f) show the eddy at 90° phase, (g)-(i) show the eddy at 180° phase, (j)-(l) show the eddy at 270° phase. The left column shows local vorticity in color (anti-cyclonic in green, cyclonic in red); the middle column shows surface layer depth in color (lighter is shallower, darker is deeper); the right column shows vorticity (purple is greater). Over the Central American Rise the depth (middle column) reaches a maximum of only 100m and as a result the PV (right column) is particularly high there. Note that PV is always positive due to the importance of planetary vorticity. supplemental video 1 shows an animation of this figure.

Accepted for publication in *Journal of Physical Oceanography*. DOI 10.1175/JPO-D-24-0049.1.

The evolution of an average Caribbean Current eddy is visible in Figure 3 in the northern part of the domain. At 0° phase, a negative ζ, deep surface layer, positive SSH signal is visible in two locations in the northwestern Caribbean Sea (Figure 3a-c), one near 80° W and one near 74° W. The phase-average is with respect to the eddy at 74° W; the other location is a remnant eddy, the previous one to pass through the domain. By 90° phase (Figure 3d-f), the remnant eddy has dissipated or been advected into the Cayman Basin (to the northwest of the domain shown in Figure 3), while the eastern eddy has propagated to the west. This propagation continues through 180° phase (Figure 3g-i), when the strong westward currents in the south part of the eddy begin to make contact with the Central American Rise. The flow splits around the Rise's shallow topography (see 80 to 82 $^{\circ}W$, 12 to 15 $^{\circ}N$), and this flow branching intensifies as the eddy continues to propagate west through 180° phase (Figure 3g-i) and maintains strength through 270° phase (Figure 3j-l, supplemental video 1). This branching of flow around the Central American Rise appears to cause PV fluxes into the PCG region (Figure 4a), altering the gyre's structure and the region's coastal currents. A mechanistic description of the flow branching process is beyond the scope of this work, but the process has been described using different methodology in Andrade and Barton (2000) and Hughes et al. (2016), and is clearly visible in Figure 3 and supplemental videos 1 & 2. The PV flux associated with the flow branching process is the negative PV flux along the western side of the control volume's northern boundary (Figure 4a), which intensifies between 180° and 270° phase. Near the end of the phase-averaging period, the next eddy enters the domain from the east.

The Panamá-Colombia Gyre has, on average, positive local vorticity (cyclonic), a shallow surface layer depth, and negative SSH, leading to strongly positive PV due to the additional influence of the planetary component (equation 1). The gyre is a stationary feature that changes structure as Caribbean Current eddies propagate to its north. Generally, the gyre's southern, eastward branch (the CCC) is stronger and longer in extent than its northern, westward branch, as the northern branch shrinks around 90 ° phase (Figure 3 third column, Andrade et al. (2003); Correa-Ramirez et al. (2020); Orfila et al. (2021)). In the parlance of the gyre modes introduced in section 1, this is a transition from mode (A) to mode (B).

The gyre's evolution in response to the variability in PV fluxes over the course of a Caribbean Current eddy period is apparent in Figure 3 in the southern part of the domain. At 0° phase (Figure 3a-c), the gyre appears as a region of positive local vorticity and shallower surface layer depth

Accepted for publication in *Journal of Physical Oceanography*. DOI 10.1175/JPO-D-24-0049.1.

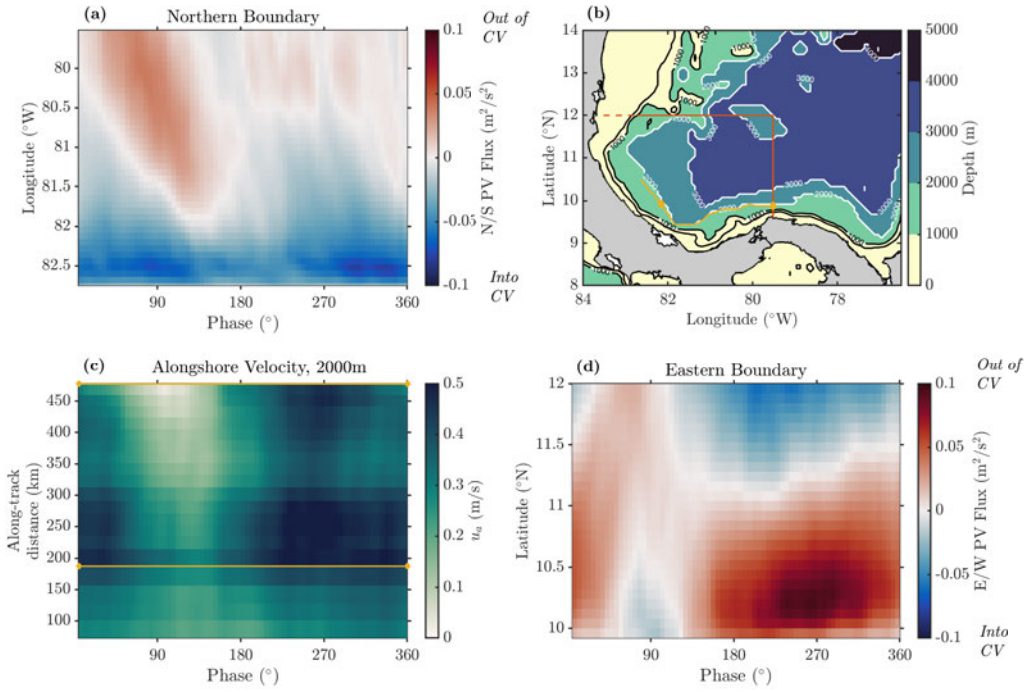

FIG. 4: Phase-averaged PV fluxes and currents into and within the PCG region. Panel (a) shows the phase-averaged meridional PV flux through the northern boundary shown in (b) and Figure 1. Small PV fluxes through this boundary west of 82.75 °W (the dashed portion of the northern control volume boundary in panel b) over the Central American Rise are not shown. Panel (b) shows a map of the southwest Caribbean Sea, with colored contours at 1000m intervals and black contours at 500 m and 1000m. The orange lines shown are the same as on Figure 1 and show the open control volume boundaries used to calculate the PV balance in equation 7 in sections 2c and 3b. The dashed portion of the northern boundary indicates the section over the Central American Rise. The gold line shows the representative location of the transect along which alongshore velocity is shown in panel (c); the gold diamonds indicate the locations of the currents shown in Figure 5 offshore of Bocas (westward most diamond) and offshore of Colon (eastward most diamond). Panel (c) shows the major axis component of phase-averaged surface layer currents between the 1800 and 2200m isobaths, calculated using a principal axis rotation (Emery and Thomson 1998). Along-track distance is measured along the gold line in panel b, starting from the west and progressing eastward. Panel (d) shows the phase-averaged zonal PV flux through the eastern boundary shown in (b) and Figure 1. All calculated values of PV are positive, so the sign of the flux on panels (a) and (d) is solely determined by the sign of the velocity.

off of the northern coast of Panamá, with the gyre's eastward velocities causing a positive PV flux through most of the eastern CV boundary (Figure 4d). In the Darien Gulf, there is a region of negative (anti-cyclonic) local vorticity that extends westward north of the Isthmus of Panamá, joining with the coastal boundary layer. This feature propagates north-westward, and by 90° phase is located just north of Colón at the Isthmus of Panamá (Figure 3d-f), having split the gyre into two regions of positive vorticity separated by a region of negative local vorticity (gyre mode D in 1). This region of negative local vorticity is associated with a northward PV flux across the northern CV boundary and a westward PV flux across the eastern CV boundary (Figure 4a,d). As

Accepted for publication in *Journal of Physical Oceanography*. DOI 10.1175/JPO-D-24-0049.1.

the Caribbean Current eddy to the north begins to make contact with the Central American Rise at 180° phase (Figure 3g-i), the region of positive vorticity has joined again (gyre mode A in 1), and its strength increases between 180 and 270° phase (Figure 3j-l) as the region of PV fluxes into the northern and out of the eastern boundaries grows (Figure 4a,d). At this point, the region of negative vorticity in the Darien Gulf has begun to re-form, and the cycle starts anew.

Supplemental video 2 shows the daily surface layer average vorticity, velocity vectors, and sea surface height contours over the entire 22 year HYCOM run. While there are differences between the eddy-averaged picture presented above at any point in the time series shown in supplemental video 2, the dynamics of the eddy average are clearly visible for most eddy passage events, including the deflection of the Caribbean Current to the south, the associated increase in energy of the Panamá-Colombia Gyre, and the related flow separation at the Isthmus of Panamá and spinup of the Darien Gulf vortex.

The Caribbean Coastal Countercurrent strength, therefore, also varies with eddy phase. Alongshore currents along the gold line on Figure 4b (close to the 2000m isobath) are shown on Figure 4c. For this descriptive analysis only, the alongshore component of the surface layer average velocity was estimated as the major axis component of phase-averaged surface layer currents between the 1800 and 2200m isobaths, calculated using a principal axis rotation (Emery and Thomson 1998). The fastest currents at all longitudes occur near 270° phase. Similarly, the minimum value occurs near 100° phase. The range between minimum and maximum is not constant with longitude, but increases monotonically from 0.13 m/s to 0.44 m/s along the line eastward. This analysis demonstrates that Caribbean Current eddies can modify coastal currents hundreds of kilometers away—changing their magnitude by 50%. (Figure 4b). This is also seen in the alongshore currents at Bocas and Colon shown on Figure 5a. We show in the next section that this coastal current variability is related to the eddy phase-averaged absolute PV balance.

b. Eddy vorticity balance

We evaluate the phase-averaged PV balance described in sections 2c-d and equation 7 over the control volume (CV) region enclosed by the orange lines in Figures 1 and 4b. We remind the reader that the effect of the phase-average is to characterize the signal related to the passage of an average Caribbean Current eddy across the northern part of the basin. Variability in the phase-averaged PV

Accepted for publication in *Journal of Physical Oceanography*. DOI 10.1175/JPO-D-24-0049.1.

budget terms is therefore due primarily to Caribbean Current eddy influence. The PV fluxes at the boundary of this region consist of meridional PV transport through the northern boundary, located at 12 °N, and zonal PV transport at the eastern boundary, located at -79.5°W. The cross-sectionally integrated meridional fluxes through the northern CV boundary are always negative, as positive PV is advected southward into the PCG region. Similarly, the cross-sectionally integrated zonal fluxes through the eastern CV boundary are always positive, as positive PV is advected eastward out of the PCG region. The wind stress curl influence on the PV balance is integrated over the area defined by the coastline and the offshore boundaries marked in orange on Figure 1 and 4b, and the PV storage term is taken over the surface layer depth (H) and the same area. This storage term is near zero and not shown on Figure 5b for clarity. Phase-averaged meridional and zonal PV fluxes, wind stress curl, and residual PV flux are shown over the eddy phase cycle on Figure 5b.

Cross-sectionally integrated meridional eddy phase-averaged PV fluxes into the PCG region (blue line on Figure 5b) vary in magnitude, from -0.08 m^2/s^2 at their weakest (110 ° phase) to -1.1 m^2/s^2 at their strongest (305 ° phase). The minimum flux magnitude occurs after the eddy has dissipated or has moved into the Cayman basin (Figure 3b & d), and the maximum flux magnitude occurs when the eddy impacts the Central American Rise. The interaction of Caribbean Current eddies with the Central American Rise outlined in section 3a appears to influence these meridional fluxes, as is also supported by the findings of Andrade and Barton (2000) and Hughes et al. (2016). This process is visible in supplemental videos 1, 2, & 3.

We observe similar variability in the cross-sectional integrated zonal PV fluxes (orange line on Figure 5b), which approach zero at their weakest (115 ° phase) and 0.73 m^2/s^2 at their strongest (310 ° phase). Zonal PV fluxes through the eastern boundary are therefore nearly in phase with meridional PV fluxes through the northern boundary, although their magnitude is smaller. We again note that PV storage in the PCG region is small, so this imbalance must indicate an input of negative PV or a loss of PV in the region.

The PV flux due to the wind stress curl (purple line on Figure 5b) integrated over the region's surface is uncorrelated with the eddy cycle and is therefore an effectively constant PV source over the average eddy period. Variability in wind stress over the PCG region is thus not a primary driver of oscillations over the eddy cycles (T_{eddy} = 116 days, section d); however, larger scale winds

Accepted for publication in *Journal of Physical Oceanography*. DOI 10.1175/JPO-D-24-0049.1.

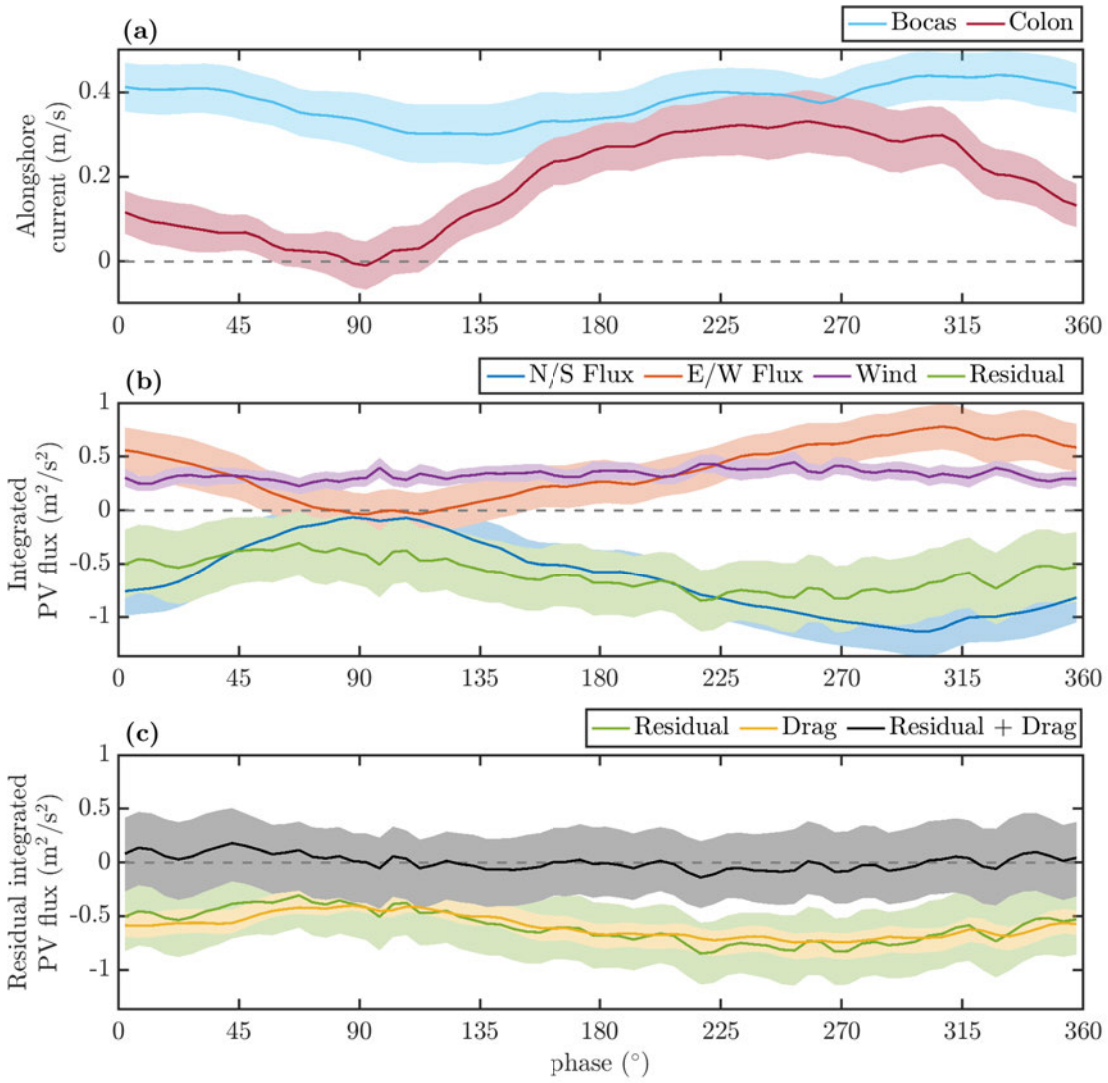

FIG. 5: Plots of phase-averaged currents and PV balance terms with respect to eddy phase. Shaded regions represent the 95% confidence interval on all panels. Panel (a) shows the alongshore components of phase-averaged velocity at Bocas del Toro and Colón, the western and eastern gold diamonds shown on Figure 4b, respectively. Panel (b) shows the phase-averaged PV balance terms from equation 7 with respect to phase; the green line is the sum of the terms on the left hand side of equation 7. Panel (c) shows the portion of this residual that can be explained by drag calculated as described in sections 2c and 3b in yellow; the near-zero remaining, unexplained portion is shown in dark grey.

may play a role in generating Caribbean Current eddies through baroclinic instability processes (Andrade and Barton 2000; Jouanno et al. 2008; Orfila et al. 2021).

We calculate a residual PV flux (green line on Figure 5b) by summing the PV storage, PV flux, and wind stress curl terms on the left hand side of equation 7 (noting again that PV storage is

Accepted for publication in *Journal of Physical Oceanography*. DOI 10.1175/JPO-D-24-0049.1.

near zero). This residual PV flux is always negative, indicating that the terms included on the left hand side of equation 7 do not sum to zero in the PCG region. The residual's magnitude increases between 105° and 220° phase, changing from -0.35 m^2/s^2 to -0.82 m^2/s^2. This variability is in phase with both the PV fluxes and the currents shown in Figure 5a. This net negative residual PV flux indicates that an PV sink is required in the region to close the PV balance. The residual PV flux is larger when the currents in the region are larger, indicating that friction is likely important to this process.

Following the linear model of drag introduced in section 2c, we assume that the residual PV flux is largely due to friction, and we can correspondingly calculate the linear drag coefficient $r_c = 8.77 \pm 0.97 \times 10^{-5}$ s^{-1} (the results of this fit are shown on Figure 6). The fit is significant ($p < 0.0001$ for r_c) and explains much of the variance observed in the residual of the PV budget discussed above ($R^2 = 0.82$). The linear drag coefficient obtained from equation 7 is in line with literature values, which range from $10^{-6} < r_c < 10^{-4}$ s^{-1} (Yang and Price 2000; Chang and Oey 2011). While we will use this interpretation of the residual as being driven by drag throughout the rest of this work, we note here that the residual also includes error introduced by the assumptions made in our control volume, phase-averaged approach and unresolved physical mechanisms.

The y-intercept of the linear model of drag ($C = 0.17 \pm 0.09$ m^2/s^2, $p = 0.00013$) can be related to the average effect of interfacial friction at the base of the surface layer along the domain's open boundaries as outlined in section 2c, using the along-path component of the velocity along the cubic-spline fit path shown on figure 1. Using equation 6, we calculate $0 < r_o < 4.9 \times 10^{-6}$ s^{-1}, propagating uncertainty in both C and the integrated open boundary velocity ($\overline{u}_{open} = 0.15 \pm 0.02$ m/s, 95% confidence interval given, integrated over 589 km). This range includes the possibility that interfacial drag is not important, a common assumption in potential vorticity balances (Rhines 1986). On the upper end of the range of r_o, its value is still ~ 20 times smaller than the value of r_c, the value calculated above for coastal friction. We note that r_c is of the right order of magnitude given the HYCOM quadratic bottom drag coefficient ($C_D = 5 \times 10^{-3}$), the water depth along the coastal boundary, and the coastal velocities. As outlined in section 2c, we expect that r_c is slightly elevated due to the influence of horizontal turbulent transport, which like bottom drag will vary in phase with the along-coast velocity. We will therefore interpret these results as the total impact of drag (vertical and horizontal) related to the in-phase variability of the along-coast velocity.

Accepted for publication in *Journal of Physical Oceanography*. DOI 10.1175/JPO-D-24-0049.1.

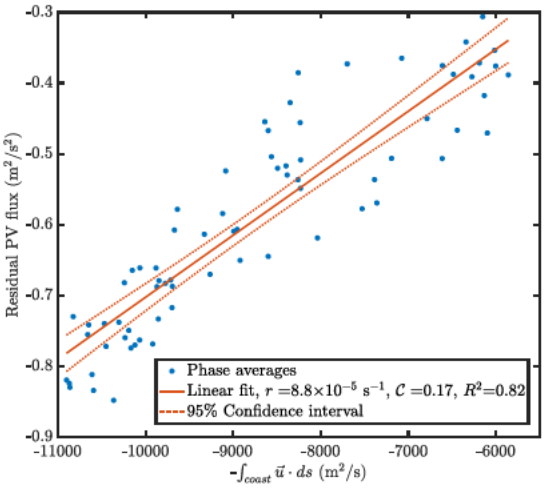

FIG. 6: Linear fit of the residual PV flux shown in Figure 5b to the path integral of velocity along the coast. Blue dots show each 5° phase bin. The solid orange line shows the fit ($R^2 = 0.82$), which yields a slope of $r = 8.77 \pm 0.9 \times 10^{-5}$ s^{-1} ($p < 0.0001$), and a y-intercept of $C = 0.17 \pm 0.09$ m^2/s^2 ($p = 0.0014$) while the dashed orange lines show the 95% confidence interval on the fit.

As our calculations of r_c and r_o are defined as constant in time, the phase evolution of the drag term shown on Figure 5c is due solely to changes in the coastal currents, as described in section 3a. Adding the drag to the residual PV flux yields a new friction-inclusive residual PV flux (black line on Figure 5c) that is near zero and does not vary significantly over the period of an average eddy. Thus, the PV balance in the PCG region is represented well by a simple balance of PV fluxes, wind stress curl, and friction along the coastal boundary. Caribbean Current eddies drive significant variability in PV fluxes, which are in a quasi-steady balance with friction along the coastal boundary.

4. Seasonal variability and coastal current reversals

We have shown that Caribbean Current eddies can significantly change the structure of the Panamá-Colombia Gyre and the coastal currents in the southwest Caribbean sea. As noted in section 1, changes to these currents will have important impacts to transport of freshwater, chemical tracers, and larvae along the coast of the southern Caribbean. We now investigate how Caribbean Current eddies influence coastal currents through seasonal variation in the PV budget, with a particular focus on the location and timing of coastal current reversals. We remind the reader that we discuss three distinct patterns of rotational flow that occur in the region: the Panama-Colombia

Accepted for publication in *Journal of Physical Oceanography*. DOI 10.1175/JPO-D-24-0049.1.

gyre, Caribbean Current eddies, and the Darien Gulf vortex, referred to exclusively as "gyre", "eddy" or "eddies", and "vortex", respectively.

The strongest east-west PV fluxes observed during an average year over the 78°W meridian (approximately in the center of the basin) occur between July and the end of September (Figure 7a). In this analysis of fluxes in the northern part of the basin, we choose the 78°W meridian due to its position west of the Central American Rise and the sills that separate the Colombian and Cayman basins of the Caribbean Sea. The time period between July and August includes both the annual maximum eastward PV flux at 78°W (in red on Figure 7a) around 10-12°N and the annual maximum westward PV flux (in blue on Figure 7a) around 12-14°N. The region of eastward flux associated with the Caribbean Coastal Countercurrent at the south end of the basin is persistent throughout the year, but separates from the coast during this time period. Similarly, the latitude of maximum westward flux (noted by the white points on Figure 7a) deflects to the south between June and August. Supplemental video 3 shows the seasonal climatology of daily surface layer average vorticity, surface layer depth, and potential vorticity overlain with velocity vectors, and sea surface height contours for the entire western Caribbean Sea region.

Intense eastward and westward Caribbean Current PV fluxes from July to September occur simultaneously with an increase in the spatially integrated north-south and east-west PV fluxes into the gyre region (Figure 7b, blue and orange lines). While the wind stress curl increases slightly during this time (Figure 7b, purple line), its contribution to the gyre PV budget remains small. We calculate drag for the annual PV budget using the linear formulation laid out in section 2c, as implemented in 3b, assuming zero PV storage. This calculation yields the drag coefficient $r_c = 8.66 \pm 0.5 \times 10^{-5}$ s^{-1} and the fitting constant $C = 0.36 \pm 0.04$ m^2/s^2. This value of r_c is nearly identical to that calculated with the phase-averaged PV budget, while the fitting constant tC has changed. The higher value of C likely indicates that the processes unresolved by the PV budget are somewhat different on yearly and eddy time scales. The fit results in an approximately closed budget (the residual is shown as the grey line on Figure 7b). The correlation of the drag (Figure 7b, yellow line) with the advective PV fluxes is consistent with the frictional balance detailed in section 3b. The eddy phase-averaged PV budget in the gyre region presented in section 3b may be conceptualized as a higher frequency perturbation driven by Caribbean Current eddies ($T_{eddy} = 116$ days, ~ 3 eddies per year) about the background seasonal climatology shown in Figure 7b, with

Accepted for publication in *Journal of Physical Oceanography*. DOI 10.1175/JPO-D-24-0049.1.

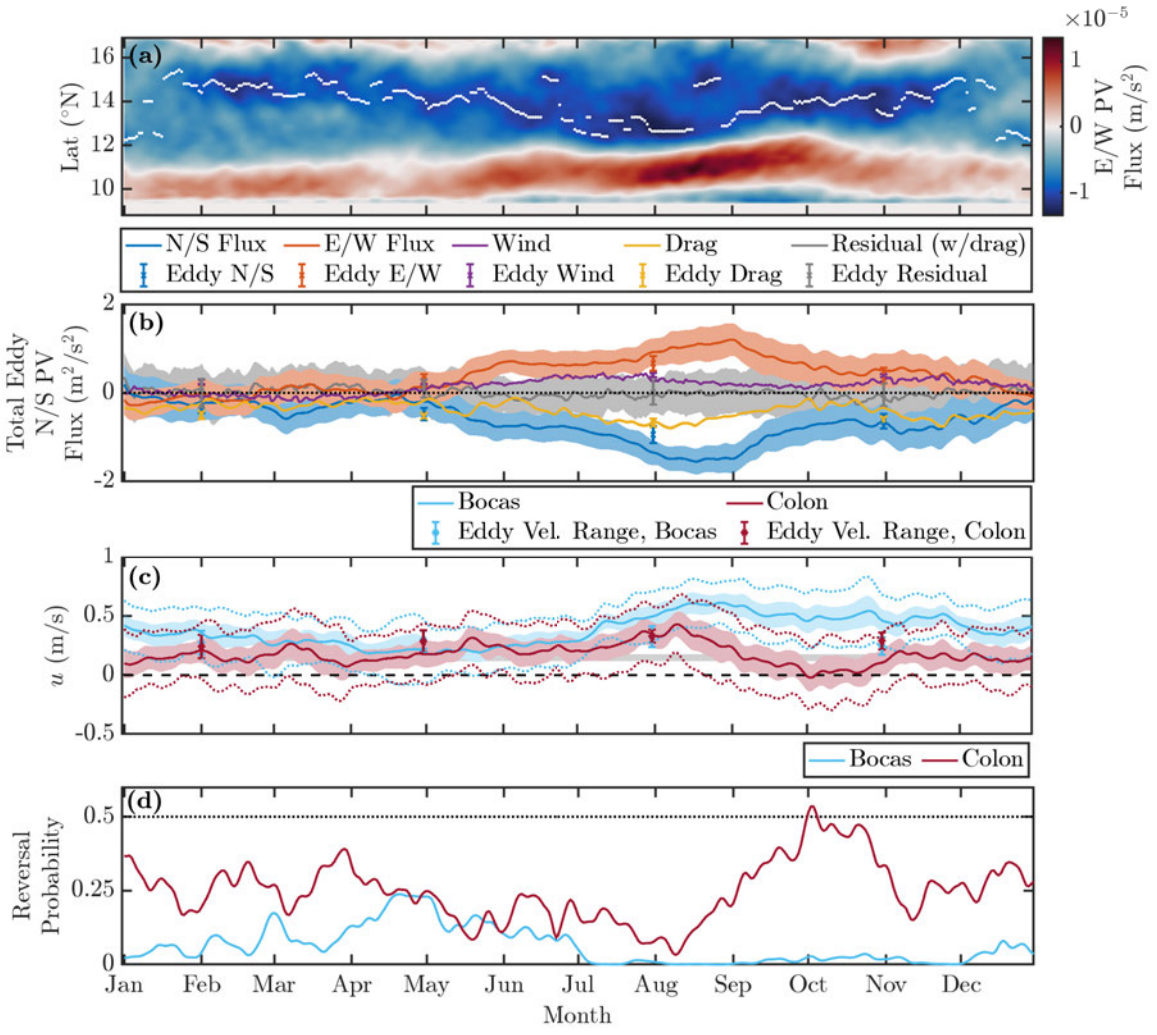

FIG. 7: Average annual values of alongshore currents, PV fluxes and balance terms, and eddy properties. Panel (a) shows the average east-west PV flux for each day of the year in color for a range of latitudes at 78°W, near the center of the dashed white line on Figure 1. Blue indicates westward PV flux, the latitude of the strongest westward PV flux is shown by a white dot for each day of the year. Panel (b) shows the same PV budget terms as Figure 5b averaged for each day of the year, with a shaded 95% confidence interval. Mean eddy event values of these same PV budget terms, bin averaged in three month windows as described in section 4, are shown as markers with 95% confidence interval error bars. The time assigned to each eddy event is the time when half of the event's total PV flux has passed through the northern boundary of the control volume shown in Figures 1 and 4b. Panel (c) shows the average alongshore current for each day of the year at Bocas (cyan) and Colón (burgundy) in solid lines, taken at the locations near the 2000m isobath shown in Figure 5b. The 95% confidence interval of the alongshore current for each location on each day is shown as the shaded area around each line, while the dashed lines indicates one standard deviation from the seasonal climatology on a given day. A positive current indicates roughly eastward flow, corresponding to cyclonic flow in the PCG. Markers show the average range in the alongshore currents during Caribbean Current eddy events at Bocas (cyan) and Colón (burgundy) for the three month bins; error bars on these markers indicate the 95% confidence interval. Panel (d) shows the probability of a velocity reversal (negative current on panel c) on a given day of the year calculated as described in section 4

Accepted for publication in *Journal of Physical Oceanography*. DOI 10.1175/JPO-D-24-0049.1.

the same balance of advective PV flux and friction explaining variability on each time scale. The average eddy PV flux oscillation amplitude presented in section 3b is roughly half as large in amplitude as the background seasonal oscillation in terms of advective PV flux (Figure 5b). We note that care must be taken in interpreting results in this manner, as the eddy phase-average is calculated with respect to phase, rather than time.

The coastal currents at Colón and Bocas del Toro are generally consistent with the cyclonic flow of the PCG (approximately eastward). During the intensification of the coastal currents near Bocas del Toro, the main trunk of the Caribbean Current is at its most intense and furthest south. Between the months of January and August, the coastal currents along the northern coast of Panamá at Bocas del Toro and Colón (using the same locations shown on Figure 4b) have similar velocity magnitudes, both increasing in August (Figure 7a). At this point, the mean current at Colón decreases in magnitude sharply compared to Bocas, similar to the structure of these currents at 90° eddy phase (Figure 5a), when local vorticity in the Darien Gulf is negative as an anti-cyclonic vortex propagates northwestward (section 3a). The current at Colón recovers to a similar magnitude to Bocas by November.

To assess whether the seasonal variability in Caribbean Current eddy dynamics influences the yearly mean PV balance, we will examine the PV balance outlined in sections 2c and 3b for each Caribbean Current eddy detected, and seasonally average the results. We subsequently refer to the detection of a Caribbean Current eddy in the northern part of the basin as an "eddy event". Each eddy event is first assigned a characteristic time stamp, defined as the time for a given eddy event at which the cumulative north-south PV flux into the gyre region control volume (shown on Figures 1 and 4b) has reached half of its total for that eddy event. For each eddy event, we calculate the mean north-south (east-west) PV flux through the northern (eastern) boundary of the control volume, the mean wind-driven PV flux, the sum of these mean PV budget terms, and the range in the alongshore coastal current near Bocas del Toro and Colón at the points shown on Figure 4b. The eddy events are then separated into three-month bins: 14 eddy events occur between January and March, 13 between April and June, 23 between July and September, and 16 between October and December. The mean of the quantities outlined above in these bins are shown as markers with 95% confidence interval error bars on Figure 7b and c. These calculations yield bulk properties that are taken in a time-mean sense, rather than a phase-mean sense.

Accepted for publication in *Journal of Physical Oceanography*. DOI 10.1175/JPO-D-24-0049.1.

The larger number of eddy events identified in the summer months suggests that conditions are more favorable for eddies to form, or that the eddy event duration is shorter, between July and September. A χ^2 test does not find the larger number of eddies in July-September to be significant ($\chi^2 = 3.697$, $\chi^2_{\alpha=0.05,df=3} = 7.815$, $p = 0.296$); however, the sample size is somewhat small (66 eddies). Further study, and a longer time series, is required for any conclusions about seasonal aliasing in the seasonal climatology PV balance due to preferential eddy formation to be drawn. Therefore, we do not consider seasonal aliasing in eddy formation or eddy event duration in the subsequent analysis.

There are seasonal patterns in the variability of coastal currents in the southwest Caribbean Sea. These patterns of variability include reversals in the coastal current, when flow is directed opposite to the normal anti-cyclonic rotation of the PCG (Figure 7c, d). This seasonal variability is consistent with a modest observed increase in the range of alongshore currents during Caribbean Current eddy events from January to July. The frequency of reversals at Bocas del Toro and Colón also varies with the annual cycle (Figure 7d). The reversal frequency is calculated using the normal distribution defined by the mean and standard deviation of the alongshore current for that day as shown in figure 7c. Coastal current variability is slightly larger throughout most of the year at Colón than at Bocas, with more frequent flow reversals, especially in the last half of the year.

We note the proximity of the Colón site (Figure 4b) to Darien Gulf. The formation and strength of the Darien Gulf anti-cyclonic vortex described in section 3a and shown on Figure 3a & d (as well as all supplemental videos) may play a role in altering the range of the currents at the eastern edge of the control volume. Stronger alongshore currents may lead more intense vortices to be shed off the isthmus of Panamá, changing the range of currents at Colón. Future work should seek to understand the dynamics that govern the formation and separation of this Darien Gulf vortex.

As shown above for the seasonal climatology values, an increase in mean southward eddy event PV flux into the control volume during the summer months (Figure 7c, blue markers) occurs simultaneously with a corresponding increase in the magnitude of mean eastward eddy event PV flux out of the control volume (Figure 7c, orange markers). The mean eddy event wind PV input does not vary much over the course of the year (Figure 7c, purple markers). This results in a $\sim 30\%$ increase of mean eddy event drag loss of PV in the summer months (Figure 7c, yellow markers).

Accepted for publication in *Journal of Physical Oceanography*. DOI 10.1175/JPO-D-24-0049.1.

Therefore, increases in westward Caribbean Current PV flux between July and September are associated with larger magnitude eddy event PV fluxes in the PCG region.

The increase in mean eddy event PV flux as the westward PV flux in the Caribbean current increases and moves south from July-September indicates that Caribbean Current eddies can effectively transport Caribbean Current eddy PV southward. Therefore, the energy state of the Caribbean Current may in part determine the mean PV advected south by the eddies (Figure 7b). The heightened PV fluxes during the summer months are associated with a modest increase in the mean range of alongshore coastal currents during eddy events. Importantly, the average values of PV flux vary similarly over one eddy period (Figures 5b and 7d) and one year (Figure 7c). This implies that eddy dynamics have the potential to alter dynamics by a similar amount to seasonal variability over a time scale that is one-third as long ($T_{eddy} \approx 116$ days).

As mean coastal current range over eddy events varies only modestly with the mean PV flux over the seasonal cycle, eddies that occur when the system is in a lower energy state (November to June) may have a larger relative effect on the alongshore currents. The mean range of currents during eddy events at Bocas (Figure 7c) is strong enough to reverse the direction of the alongshore current (Figure 7a) with some frequency during times outside the summer intensification period, especially in the months of April-June (Figure 7d). At Colón, the mean range of currents during eddy events is strong enough to reverse the flow direction throughout most of the year, with a minimum reversal probability occurring with the peak of alongshore flow in August (Figure 7d). The seasonality of these reversals may have important impacts for local dynamics and coastal ecosystems, and future work should investigate the specific physical mechanisms that link Caribbean Current eddies to coastal current reversals on the southern edge of the southwest Caribbean Sea.

5. Summary

Using 22 years of HYCOM output, we show that eddies advected by the Caribbean Current along the Caribbean Sea's northern boundary influence the coastal currents along the Caribbean basin's southwest coast. PV fluxes into the Panamá-Colombia Gyre region occur as these eddies interact with the Central American Rise. The increase in PV fluxes is balanced by an increase in drag (with a linear drag coefficient of $r_c = 8.77 \pm 0.97 \times 10^{-5}$ s^{-1}), with a corresponding increase in local alongshore currents. Alongshore currents near Bocas del Toro and Colón vary by 0.15 and 0.5

Accepted for publication in *Journal of Physical Oceanography*. DOI 10.1175/JPO-D-24-0049.1.

m/s respectively over the course of an average eddy passage. The strong coastal currents at Colon precede the formation of an anticyclonic vortex in the Darien Gulf that is shed and propagates back into the gyre region as the PV flux weakens, with a coincident decrease in coastal current velocities until the next eddy passage event.

The local coastal currents are more intensely eastward between July and October at Bocas del Toro, suggesting that eddy-driven current reversals at Bocas mostly occur between December and July. At Colón, however, eastward velocities are weakest between August and October, and therefore eddy activity during this time can preferentially lead to alongshore current reversals near the Isthmus of Panamá. Coastal currents in the southwest Caribbean feed the upwelling system offshore of La Guajira peninsula (Correa-Ramirez et al. 2020; Orfila et al. 2021), suggesting that eddy influence may be important for understanding variability in that system. These findings reveal pathways for connectivity between the Caribbean Current eddy field and coastal currents in the southwest Caribbean Sea.

Acknowledgments. We would like to thank Dr. Shuwen Tan for discussion and feedback that was critical to this work, along with the editorial work of Dr. Jacob Wenegrat and two anonymous reviewers. Collaborative NSF grants OCE-1924664, OCE-1924220, and OCE-19424551 funded this project. Fieldwork for a related project was conducted at the Smithsonian Tropical Research Institute Bocas del Toro field station; the authors would like to specifically acknowledge the help of Ximena Boza, Viviana Bravo, Carolina Cesar, and Plinio Gondola on site.

Data availability statement. All data presented here (including NCEP meterological forcing) can be downloaded from the HYCOM data portal at the following link: https://www.hycom.org/data/glbv0pt08/expt-53ptx

References

Andrade, C. A., and E. D. Barton, 2000: Eddy development and motion in the Caribbean Sea. *Journal of Geophysical Research: Oceans*, **105 (C11)**, 26 191–26 201, https://doi.org/10.1029/2000JC000300, URL https://onlinelibrary.wiley.com/doi/abs/10.1029/2000JC000300, _eprint: https://onlinelibrary.wiley.com/doi/pdf/10.1029/2000JC000300.

Andrade, C. A., E. D. Barton, and C. N. K. Mooers, 2003: Evidence for an eastward flow along the Central and South American Caribbean Coast.

Accepted for publication in *Journal of Physical Oceanography*. DOI 10.1175/JPO-D-24-0049.1.

Journal of Geophysical Research: Oceans, **108 (C6)**, https://doi.org/10.1029/2002JC001549, URL https://onlinelibrary.wiley.com/doi/abs/10.1029/2002JC001549, _eprint: https://onlinelibrary.wiley.com/doi/pdf/10.1029/2002JC001549.

Arzeno, I. B., S. N. Giddings, G. Pawlak, and R. Pinkel, 2020: Generation of quasi-biweekly yanai waves in the equatorial indian ocean. *Geophysical Research Letters*, **47 (16)**, e2020GL088 915, https://doi.org/https://doi.org/10.1029/2020GL088915, URL https://agupubs.onlinelibrary.wiley.com/doi/abs/10.1029/2020GL088915, e2020GL088915 10.1029/2020GL088915, https://agupubs.onlinelibrary.wiley.com/doi/pdf/10.1029/2020GL088915.

Bretherton, C. S., and C. Schär, 1993: Flux of potential vorticity substance: A simple derivation and a uniqueness property. *Journal of the Atmospheric Sciences*, **50**, 1834–1834.

Brokaw, R. J., B. Subrahmanyam, and S. L. Morey, 2019: Loop Current and Eddy-Driven Salinity Variability in the Gulf of Mexico. *Geophysical Research Letters*, **46 (11)**, 5978–5986, https://doi.org/10.1029/2019GL082931, URL https://onlinelibrary.wiley.com/doi/abs/10.1029/2019GL082931, _eprint: https://onlinelibrary.wiley.com/doi/pdf/10.1029/2019GL082931.

Brooks, D. A., and D. W. Townsend, 1989: Variability of the coastal current and nutrient pathways in the eastern gulf of maine. *Journal of Marine Research*, **47 (2)**, 303–321.

Centurioni, L. R., and P. P. Niiler, 2003: On the surface currents of the caribbean sea. *Geophysical Research Letters*, **30 (6)**, https://doi.org/https://doi.org/10.1029/2002GL016231, URL https://agupubs.onlinelibrary.wiley.com/doi/abs/10.1029/2002GL016231, https://agupubs.onlinelibrary.wiley.com/doi/pdf/10.1029/2002GL016231.

Chang, Y.-L., and L.-Y. Oey, 2011: Loop current cycle: Coupled response of the loop current with deep flows. *Journal of Physical Oceanography*, **41 (3)**, 458 – 471, https://doi.org/10.1175/2010JPO4479.1, URL https://journals.ametsoc.org/view/journals/phoc/41/3/2010jpo4479.1.xml.

Chassignet, E. P., H. E. Hurlburt, O. M. Smedstad, G. R. Halliwell, P. J. Hogan, A. J. Wallcraft, R. Baraille, and R. Bleck, 2007: The hycom (hybrid coordinate ocean model) data assimilative system. *Journal of Marine Systems*, **65 (1)**, 60–83, https://doi.org/https:

Accepted for publication in *Journal of Physical Oceanography*. DOI 10.1175/JPO-D-24-0049.1.

//doi.org/10.1016/j.jmarsys.2005.09.016, URL https://www.sciencedirect.com/science/article/pii/S0924796306002855, marine Environmental Monitoring and Prediction.

Correa-Ramirez, M., a. Rodriguez-Santana, C. Ricaurte-Villota, and J. Paramo, 2020: The Southern Caribbean upwelling system off Colombia: Water masses and mixing processes. *Deep Sea Research Part I: Oceanographic Research Papers*, **155**, 103 145, https://doi.org/10.1016/j.dsr.2019.103145, URL https://www.sciencedirect.com/science/article/pii/S0967063719302912.

Cowen, R. K., C. B. Paris, and A. Srinivasan, 2006: Scaling of connectivity in marine populations. *Science*, **311 (5760)**, 522–527, https://doi.org/10.1126/science.1122039, URL https://www.science.org/doi/abs/10.1126/science.1122039, https://www.science.org/doi/pdf/10.1126/science.1122039.

Cummings, J. A., 2005: Operational multivariate ocean data assimilation. *Quarterly Journal of the Royal Meteorological Society*, **131 (613)**, 3583–3604, https://doi.org/https://doi.org/10.1256/qj.05.105, URL https://rmets.onlinelibrary.wiley.com/doi/abs/10.1256/qj.05.105, https://rmets.onlinelibrary.wiley.com/doi/pdf/10.1256/qj.05.105.

Cummings, J. A., and O. M. Smedstad, 2013: *Variational Data Assimilation for the Global Ocean*, 303–343. Springer Berlin Heidelberg, Berlin, Heidelberg, https://doi.org/10.1007/978-3-642-35088-7_13, URL https://doi.org/10.1007/978-3-642-35088-7_13.

Doblin, M. A., and E. van Sebille, 2016: Drift in ocean currents impacts intergenerational microbial exposure to temperature. *Proceedings of the National Academy of Sciences*, **113 (20)**, 5700–5705, https://doi.org/10.1073/pnas.1521093113, URL https://www.pnas.org/doi/abs/10.1073/pnas.1521093113, https://www.pnas.org/doi/pdf/10.1073/pnas.1521093113.

Emery, W. J., and R. E. Thomson, 1998: *Data Analysis Methods in Physical Oceanography*. Pergamon Press.

Gaube, P., and D. J. McGillicuddy, 2017: The influence of Gulf Stream eddies and meanders on near-surface chlorophyll. *Deep Sea Research Part I: Oceanographic Research Papers*, **122**, 1–16, https://doi.org/10.1016/j.dsr.2017.02.006, URL https://www.sciencedirect.com/science/article/pii/S0967063715300868.

Accepted for publication in *Journal of Physical Oceanography*. DOI 10.1175/JPO-D-24-0049.1.

Harvey, M. E., S. N. Giddings, G. Pawlak, and J. A. Crooks, 2023: Hydrodynamic variability of an intermittently closed estuary over interannual, seasonal, fortnightly, and tidal timescales. *Estuaries and Coasts*, **46 (1)**, 84–108.

Haynes, P. H., and M. E. McIntyre, 1987: On the evolution of vorticity and potential vorticity in the presence of diabatic heating and frictional or other forces. *Journal of Atmospheric Sciences*, **44 (5)**, 828–841.

Hickey, B., S. Geier, N. Kachel, and A. MacFadyen, 2005: A bi-directional river plume: The columbia in summer. *Continental Shelf Research*, **25 (14)**, 1631–1656, https://doi.org/https://doi.org/10.1016/j.csr.2005.04.010, URL https://www.sciencedirect.com/science/article/pii/S0278434305000786.

Hickey, B., A. MacFadyen, W. Cochlan, R. Kudela, K. Bruland, and C. Trick, 2006: Evolution of chemical, biological, and physical water properties in the northern california current in 2005: Remote or local wind forcing? *Geophysical Research Letters*, **33 (22)**, https://doi.org/https://doi.org/10.1029/2006GL026782, URL https://agupubs.onlinelibrary.wiley.com/doi/abs/10.1029/2006GL026782, https://agupubs.onlinelibrary.wiley.com/doi/pdf/10.1029/2006GL026782.

Horner-Devine, A. R., R. D. Hetland, and D. G. MacDonald, 2015: Transport and mixing in coastal river plumes. *Annual Review of Fluid Mechanics*, **47**, 569–594.

Huang, M., X. Liang, Y. Zhu, Y. Liu, and R. H. Weisberg, 2021: Eddies Connect the Tropical Atlantic Ocean and the Gulf of Mexico. *Geophysical Research Letters*, **48 (4)**, e2020GL091 277, https://doi.org/10.1029/2020GL091277, URL https://onlinelibrary.wiley.com/doi/abs/10.1029/2020GL091277, _eprint: https://onlinelibrary.wiley.com/doi/pdf/10.1029/2020GL091277.

Hughes, C. W., J. Williams, A. Hibbert, C. Boening, and J. Oram, 2016: A Rossby whistle: A resonant basin mode observed in the Caribbean Sea. *Geophysical Research Letters*, **43 (13)**, 7036–7043, https://doi.org/10.1002/2016GL069573, URL https://onlinelibrary.wiley.com/doi/abs/10.1002/2016GL069573, _eprint: https://onlinelibrary.wiley.com/doi/pdf/10.1002/2016GL069573.

Jouanno, J., J. Sheinbaum, B. Barnier, and J.-M. Molines, 2009: The mesoscale variability in the Caribbean Sea. Part II: Energy sources. *Ocean Modelling*, **26 (3)**, 226–239,

Accepted for publication in *Journal of Physical Oceanography*. DOI 10.1175/JPO-D-24-0049.1.

https://doi.org/10.1016/j.ocemod.2008.10.006, URL https://www.sciencedirect.com/science/article/pii/S1463500308001601.

Jouanno, J., J. Sheinbaum, B. Barnier, J. M. Molines, and J. Candela, 2012: Seasonal and interannual modulation of the eddy kinetic energy in the caribbean sea. *Journal of Physical Oceanography*, **42 (11)**, 2041 – 2055, https://doi.org/10.1175/JPO-D-12-048.1, URL https://journals.ametsoc.org/view/journals/phoc/42/11/jpo-d-12-048.1.xml.

Jouanno, J., J. Sheinbaum, B. Barnier, J.-M. Molines, L. Debreu, and F. Lemarié, 2008: The mesoscale variability in the Caribbean Sea. Part I: Simulations and characteristics with an embedded model. *Ocean Modelling*, **23 (3)**, 82–101, https://doi.org/10.1016/j.ocemod.2008.04.002, URL https://www.sciencedirect.com/science/article/pii/S1463500308000486.

Lee, T. N., and L. P. Atkinson, 1983: Low-frequency current and temperature variability from gulf stream frontal eddies and atmospheric forcing along the southeast u.s. outer continental shelf. *Journal of Geophysical Research: Oceans*, **88 (C8)**, 4541–4567, https://doi.org/https://doi.org/10.1029/JC088iC08p04541, URL https://agupubs.onlinelibrary.wiley.com/doi/abs/10.1029/JC088iC08p04541, https://agupubs.onlinelibrary.wiley.com/doi/pdf/10.1029/JC088iC08p04541.

Lee, T. N., and E. Williams, 1999: Mean distribution and seasonal variability of coastal currents and temperature in the florida keys with implications for larval recruitment. *Bulletin of Marine Science*, **64 (1)**, 35–56.

Lin, Y., J. Sheng, and R. J. Greatbatch, 2012: A numerical study of the circulation and monthly-to-seasonal variability in the Caribbean Sea: the role of Caribbean eddies. *Ocean Dynamics*, **62 (2)**, 193–211, https://doi.org/10.1007/s10236-011-0498-0, URL https://doi.org/10.1007/s10236-011-0498-0.

Marshall, D. P., 2000: Vertical fluxes of potential vorticity and the structure of the thermocline. *Journal of physical oceanography*, **30 (12)**, 3102–3112.

McCabe, R. M., P. MacCready, and G. Pawlak, 2006: Form drag due to flow separation at a headland. *Journal of Physical Oceanography*, **36 (11)**, 2136 – 2152, https://doi.org/https://doi.

Accepted for publication in *Journal of Physical Oceanography*. DOI 10.1175/JPO-D-24-0049.1.

org/10.1175/JPO2966.1, URL https://journals.ametsoc.org/view/journals/phoc/36/11/jpo2966.1.xml.

Mooers, C. N., and G. Maul, 1998: Intra-americas sea circulation. *The sea*, **11**, 183–208.

Nidzieko, N., and S. Monismith, 2013: Contrasting seasonal and fortnightly variations in the circulation of a seasonally inverse estuary, elkhorn slough, california. *Estuaries & Coasts*, **36**, 1–17, https://doi.org/https://doi.org/10.1007/s12237-012-9548-1.

Orfila, A., C. P. Urbano-Latorre, J. M. Sayol, S. Gonzalez-Montes, A. Caceres-Euse, I. Hernandez-Carrasco, and A. G. Muñoz, 2021: On the Impact of the Caribbean Counter Current in the Guajira Upwelling System. *Frontiers in Marine Science*, **8**, URL https://www.frontiersin.org/articles/10.3389/fmars.2021.626823.

Pawlak, G., and P. MacCready, 2002: Oscillatory flow across an irregular boundary. *Journal of Geophysical Research: Oceans*, **107 (C5)**, 4–1–4–17, https://doi.org/https://doi.org/10.1029/2000JC000596, URL https://agupubs.onlinelibrary.wiley.com/doi/abs/10.1029/2000JC000596, https://agupubs.onlinelibrary.wiley.com/doi/pdf/10.1029/2000JC000596.

Pratt, L. J., G. Voet, A. Pacini, S. Tan, M. H. Alford, G. S. Carter, J. B. Girton, and D. Menemenlis, 2019: Pacific abyssal transport and mixing: Through the samoan passage versus around the manihiki plateau. *Journal of Physical Oceanography*, **49 (6)**, 1577 – 1592, https://doi.org/10.1175/JPO-D-18-0124.1, URL https://journals.ametsoc.org/view/journals/phoc/49/6/jpo-d-18-0124.1.xml.

Putman, N. F., G. J. Goni, L. J. Gramer, C. Hu, E. M. Johns, J. Trinanes, and M. Wang, 2018: Simulating transport pathways of pelagic sargassum from the equatorial atlantic into the caribbean sea. *Progress in Oceanography*, **165**, 205–214, https://doi.org/https://doi.org/10.1016/j.pocean.2018.06.009, URL https://www.sciencedirect.com/science/article/pii/S0079661118300259.

Rhines, P. B., 1986: Vorticity Dynamics of the Oceanic General Circulation. *Annual Review of Fluid Mechanics*, **18 (1)**, 433–497, https://doi.org/10.1146/annurev.fl.18.010186.002245, URL https://doi.org/10.1146/annurev.fl.18.010186.002245, _eprint: https://doi.org/10.1146/annurev.fl.18.010186.002245.

Accepted for publication in *Journal of Physical Oceanography*. DOI 10.1175/JPO-D-24-0049.1.

Richardson, P. L., 2005: Caribbean Current and eddies as observed by surface drifters. *Deep Sea Research Part II: Topical Studies in Oceanography*, **52 (3)**, 429–463, https://doi.org/10.1016/j.dsr2.2004.11.001, URL https://www.sciencedirect.com/science/article/pii/S0967064504003029.

Roughan, M., H. S. Macdonald, M. E. Baird, and T. M. Glasby, 2011: Modelling coastal connectivity in a western boundary current: Seasonal and inter-annual variability. *Deep Sea Research Part II: Topical Studies in Oceanography*, **58 (5)**, 628–644, https://doi.org/https://doi.org/10.1016/j.dsr2.2010.06.004, URL https://www.sciencedirect.com/science/article/pii/S0967064510002110, the East Australian Current – Its Eddies and Impacts.

Saha, S., and Coauthors, 2010: The ncep climate forecast system reanalysis. *Bulletin of the American Meteorological Society*, **91 (8)**, 1015 – 1058, https://doi.org/10.1175/2010BAMS3001.1, URL https://journals.ametsoc.org/view/journals/bams/91/8/2010bams3001_1.xml.

Saha, S., and Coauthors, 2014: The NCEP Climate Forecast System Version 2. *J. Climate*, **27**, 2185–2208, https://doi.org/10.1175/JCLI-D-12-00823.1.

Schiller, R., and V. Kourafalou, 2014: Loop Current Impact on the Transport of Mississippi River Waters. *Journal of Coastal Research*, **30 (6)**, 1287–1306, https://doi.org/10.2112/JCOASTRES-D-13-00025.1, URL https://doi.org/10.2112/JCOASTRES-D-13-00025.1, https://meridian.allenpress.com/jcr/article-pdf/30/6/1287/1637092/jcoastres-d-13-00025_1.pdf.

Siedlecki, S. A., N. S. Banas, K. A. Davis, S. Giddings, B. M. Hickey, P. MacCready, T. Connolly, and S. Geier, 2015: Seasonal and interannual oxygen variability on the washington and oregon continental shelves. *Journal of Geophysical Research: Oceans*, **120 (2)**, 608–633.

Stone, H. B., N. S. Banas, and P. MacCready, 2018: The effect of alongcoast advection on pacific northwest shelf and slope water properties in relation to upwelling variability. *Journal of Geophysical Research: Oceans*, **123 (1)**, 265–286, https://doi.org/https://doi.org/10.1002/2017JC013174, URL https://agupubs.onlinelibrary.wiley.com/doi/abs/10.1002/2017JC013174, https://agupubs.onlinelibrary.wiley.com/doi/pdf/10.1002/2017JC013174.

Vallis, G., 2006: *Atmospheric and Oceanic Fluid Dynamics*. Cambridge University Press, Cambridge.

Accepted for publication in *Journal of Physical Oceanography*. DOI 10.1175/JPO-D-24-0049.1.

Vasquez-Carrillo, C., and K. Sullivan Sealey, 2021: Biodiversity of upwelling coastal systems of the southern caribbean sea adjacent to guajira peninsula. *Journal of Marine Science and Engineering*, **9 (8)**, https://doi.org/10.3390/jmse9080846, URL https://www.mdpi.com/2077-1312/9/8/846.

Wilson, E. A., and S. C. Riser, 2016: An assessment of the seasonal salinity budget for the upper bay of bengal. *Journal of Physical Oceanography*, **46 (5)**, 1361 – 1376, https://doi.org/10.1175/JPO-D-15-0147.1, URL https://journals.ametsoc.org/view/journals/phoc/46/5/jpo-d-15-0147.1.xml.

Yang, J., and J. F. Price, 2000: Water-mass formation and potential vorticity balance in an abyssal ocean circulation. *Journal of Marine Research*, **58 (5)**, 789–808, https://doi.org/10.1357/002224000321358918.

Yang, Y., and Coauthors, 2019: Eddy-induced transport of saline kuroshio water into the northern south china sea. *Journal of Geophysical Research: Oceans*, **124 (9)**, 6673–6687, https://doi.org/https://doi.org/10.1029/2018JC014847, URL https://agupubs.onlinelibrary.wiley.com/doi/abs/10.1029/2018JC014847, https://agupubs.onlinelibrary.wiley.com/doi/pdf/10.1029/2018JC014847.

Yoder, J. A., L. P. Atkinson, T. N. Lee, H. H. Kim, and C. R. McClain, 1981: Role of Gulf Stream frontal eddies in forming phytoplankton patches on the outer southeastern shelf. *Limnol. Oceanogr.*, **26 (6)**, 1103–1110.

Accepted for publication in *Journal of Physical Oceanography*. DOI 10.1175/JPO-D-24-0049.1.